ELSEVIER

Behavior of lightly reinforced fiber reinforced concrete panels under pure shear loading

Luca Facconi, Fausto Minelli*

Department of Civil, Architectural, Environmental Engineering and of Mathematics (DICATAM), University of Brescia, Italy

ABSTRACT

The load-deformation response of Fiber Reinforced Concrete (FRC) elements subjected to pure shear is still matter of strong debate within the scientific community. In this paper, the tests on six fiber reinforced concrete panels under pure shear are presented and discussed. The tests were conducted under displacement control and a peculiar loading frame was designed to ensure that a pure shear state of stress was established. Steel fibers were added in relatively low amounts (20 and 50 kg/m^3), and two steel reinforcements (0.21% and 0.74%) were selected, aiming at simulating lightly reinforced elements. A critical discussion on the influence of fibers on both global and local behavior (tension stiffening, cracking formation and propagation, post-cracking stiffness and residual strength) is presented. Finally, a novel crack spacing formulation, extended to FRC, is proposed and compared against available experimental data.

1. Introduction

The prediction of the shear behavior of Fiber Reinforced Concrete (FRC) elements still represents a challenging issue. To improve the knowledge of mechanisms related to shear, a large number of studies involving FRC members has been carried out and reported by literature.

One of the first experimental studies focusing on the shear behavior of fiber reinforced concrete beams without stirrups was performed by Li et al in 1992 [1]. It was observed that the shear strength increases in the range 100–200% when adopting a volume fraction of 1% of polyethylene, aramid or steel fibers. Later, in 1997, Adebar et al. [2] carried out tests on large-scale beams without stirrups proving that the use of a sufficient amount of fibers is able to prevent brittle shear failure in favor of a more ductile response. Lower volume fractions of steel fibers (0.5–0.75%) were adopted by Kwak et al. [3], whose tests on shear critical beams showed that the increment of the shear strength was particularly large (69–80%) especially for beams with shear span-to-depth ratios equal or lower than 2. These observations were further supported by the research carried out in 2006 by Parra-Montesinos et al. [4], who performed some shear tests on beams and then collected a database containing the results from tests performed by different researchers. The analysis of the database led to the conclusion that fibers are potentially able to replace minimum conventional shear reinforcement; anyway, the authors recommended the use of a fiber volume fraction higher than 0.75%. Unlike usual studies, Meda et al. adopted

quite low amounts (0.38–0.76%) of steel fibers to investigate the effect of fiber reinforcement on the flexural response of slender beams. The authors concluded that fibers do not significantly improve the flexural resistance and the overall ductility strongly depends on the FRC toughness over the reinforcement ratio. On the contrary, they pointed out that fibers considerably enhance the behavior of the beam at service conditions by increasing the stiffness in the cracked stage and by limiting both the deformations and crack widths. More recently, other studies [6,8] were carried out to investigate the effect of different parameters (i.e., concrete class, fiber content, mixture of different fibers and sectional height-to-width ratio) on both the shear, torsional and flexural response of FRC beams without shear reinforcement. However, in spite of this broad knowledge concerning the shear and torsion behavior of FRC beams, these latter are not suitable for studying the effects of pure shear, as flexural mechanisms cause additional in-plane actions that "disturb" the pure shear state of stress.

To better investigate membrane elements subjected to shear only, Vecchio and Collins [9] performed at the University of Toronto a series of tests on reinforced concrete panels by using a "panel element tester". The latter was specifically designed to apply in-plane monotonic loading able to simulate shear as well as combined shear and axial stress conditions. Those tests provided basic information to formulate and validate the Modified Compression Field Theory (MCFT) for reinforced concrete elements [10]. Moreover, in addition to the several tests performed on reinforced concrete elements, the same testing

---

Nomenclature

c	largest diagonal distance between any point in the concrete and a bar
d	spacing between rebars
E_{cm}	mean Young's modulus of concrete (according to Eurocode 2)
E_s	mean Young's modulus of reinforcing steel
f_{c1}	average principal tensile stress in concrete (positive quantity)
$f_{c1,cr}$	average principal tensile cracking stress in concrete
f_{c2}	average principal compressive stress in concrete (negative quantity)
$f_{c2,u}$	ultimate average principal compressive stress in concrete (negative quantity)
f_{cx}	average stress in concrete in x-direction
f_{cy}	average stress in concrete in y-direction
f_{cm}	mean cylindrical concrete compressive strength
$f_{cm,cube}$	mean cube concrete compressive strength
f_{ck}	characteristic cylindrical concrete compressive strength
f_L	mean Limit of Proportionality of FRC
f_R	mean post-cracking flexural residual strength of FRC
f_x	stress applied to the concrete panel in x-direction
f_y	stress applied to the concrete panel in y-direction
f_{sx}	average reinforcement stress in x-direction
f_{sy}	average reinforcement stress in y-direction
f_{su}	mean ultimate tensile strength of reinforcing steel
f_y	mean yielding strength of reinforcing steel
f_{yx}	mean yielding strength of reinforcing steel in x-direction
f_{yy}	mean yielding strength of reinforcing steel in y-direction
f_t	mean concrete tensile strength
$s_{m,min}$	minimum value of the average crack spacing
s_{mx}	average crack spacing in reinforced concrete relative to the x-direction
s_{my}	average crack spacing in reinforced concrete relative to the y-direction
$s_{mx,FRC}$	average crack spacing in FRC relative to the x-direction
$s_{my,FRC}$	average crack spacing in FRC relative to the y-direction
$s_{m\theta}$	average crack spacing in the concrete panel (cracks inclined at θ)
$v_{xy,cr}$	cracking shear stress relative to x-y axes
$v_{xy,max}$	maximum shear stress relative to x-y axes
v_{cxy}	shear stress in concrete relative to x-y axes
$v_{xy,u}$	ultimate shear stress relative to x-y axes
v_{xy}	shear stress relative to x-y axes
V_f	volume fraction of steel fibers
w_m	average crack width
$w_{m,max}$	maximum value of the average crack width
ε_{su}	ultimate tensile strain of reinforcing steel
ε_1	principal tensile strain in concrete (positive quantity)
ε_2	principal compressive strain in concrete (negative quantity)
ε_x	average strain in x-direction
ε_y	average strain in y-direction
$\varepsilon_{x,u}$	ultimate average strain in x-direction (panel failure)
$\varepsilon_{y,u}$	ultimate average strain in y-direction (panel failure)
θ	angle of inclintion of principal strains referred to the x-axis
$\gamma_{xy,max}$	shear strain corresponding to the maximum shear stress ($v_{xy,max}$)
$\gamma_{xy,u}$	shear strain corresponding to the ultimate shear stress ($v_{xy,u}$)
γ_{xy}	shear strain relative to x-y axes
$\gamma_{xy,cr}$	cracking shear strain relative to x-y axes
ρ_s	conventional steel reinforcement ratio
ρ_{sx}	conventional steel reinforcement ratio in x-direction
ρ_{sy}	conventional steel reinforcement ratio in y-direction
$\emptyset_x$	diameter of the bars oriented in the x-direction
$\emptyset_y$	diameter of the bars oriented in the y-direction

device has been recently used to study FRC panels containing high volume fractions of steel/polypropylene fibers (0.5–2%) in combination with a high ratio (ρ_s = 3.31%) of conventional reinforcement. In spite of its unquestionable effectiveness proved by the large number of tests performed in the last 30 years, the "panel element tester" has never been provided with a servo-controlled system to perform tests under displacement control. This fact explains its inability (see Vecchio and Collins [8], test panel PV2) to control the shear softening response typically exhibited by elements containing low conventional reinforcement ratios (ρ_s < 0.3%).

A testing device very similar to the "panel element tester" was constructed at the University of Houston in 1988 to carry out tests on membrane elements subjected to both in-plane and out-of-plane bending actions. This testing machine adopts a servo control hydraulic system that allows tests to be performed in either the strain-control mode or the load-control mode. By using the Houston panel tester, Zhang and Hsu [11] undertook a series of tests on 100 MPa reinforced concrete panels subjected to both pure shear and bi-axial tension-compression.

Bosiljkov et al. [12] adopted a simple test rig, consisting of a steel frame provided with four hinges, to perform pure shear and bi-axial loading tests on masonry panels. Compared to the more advanced panel testers of Toronto and Houston, this test rig presents a relatively simple design and it allows to carry out pure shear tests by using only one jack anchored to an external reaction frame.

Except for the quite recent FRC panels tested by Susetyo et al. [13], Carnovale and Vecchio [14] and Chasioti and Vecchio [15], no other experimental studies concerning the investigation of FRC bi-

dimensional elements under pure shear can be found in the literature. Therefore, further research is required and new useful data are needed to validate analytical models able to predict the shear response of FRC membrane elements.

Starting from the previous purpose, the present research proposes a new rig for testing either traditional reinforced concrete or FRC panels under pure shear conditions. Contrary to the quite complex panel testers above described, the test frame herein proposed is much simpler and allows to perform tests under displacement control by using an electromechanic jack as the only loading device. By using this new test frame, a total of six 820 × 820 × 50 mm panels, including two conventional reinforced concrete specimens and four FRC samples, were tested under monotonic loading. Compared to previous studies, the main novel features are related to the fiber contents and the reinforcement ratios employed. In fact, in order to provide results significant for the more widespread structural applications of FRC, two quite low volume fractions of high strength steel fibers (V_f = 0.25% − 0.63%) were considered. These two fiber dosages may represent the lower and the upper bound of fiber contents usually adopted in several structural applications (e.g., beams, elevated slabs, slab on ground, tunnel segments, etc.) widely diffused across European countries. The literature reports several experimental studies [16,18] proving that the optimal fibers contents for FRC structures are often included in the range 0.32–0.5%. Likewise other studies [19,20], steel fibers were combined with conventional rebars equally distributed in both panel directions. Two different reinforcement ratios of 0.74% and 0.21% were adopted. The latter was specifically chosen to highlight the effect of fibers in structural elements characterized by a shear softening

behavior after first cracking. It is worth remarking that these steel fiber contents and reinforcement ratios are quite common in practice but significantly lower than those generally adopted in the experimental tests reported by literature.

The results of the six experimental tests are fully reported and discussed in the following together with some considerations on the analytical prediction of crack spacing in FRC membranes.

2. Research aim and novelty

The aim of this research is to investigate the role of steel fibers in determining the shear response of panels containing low amounts (0.21% and 0.74%) of conventional reinforcement. Besides the use of low reinforcement ratios, the main novelty is represented by the adoption of an innovative simple loading frame that allows performing pure shear tests under displacement control. The latter feature is of primary importance when testing lightly reinforced elements, like those tested herein, which may be characterized by a softening response after cracking.

The research work emphasizes how FRC affects the shear response of the panels in terms of shear strength, post-cracking stiffness and tension stiffening. Moreover, an equation is proposed to predict the crack spacing of FRC elements. The proposed formulation has been validated against experimental data.

3. Experimental investigation

As mentioned above, the present work adopts a new test frame (see Section 3.2) for testing FRC panels under pure shear.

To better distinguish the specimens used in the experiments, the following designation was adopted: first index, SP for Shear Panel; second index, PC for Plain Concrete (i.e. concrete not containing fibers) and FRC for Fiber Reinforced Concrete; third index –total reinforcement ratio (ρ_s), 0.21 for $\rho_s = 0.21\%$ and 0.74 for $\rho_s = 0.74\%$; fourth index – nominal volume fraction of fibers (V_f), 0.25 for $V_f = 0.25\%$ and 0.63 for $V_f = 0.63\%$.

3.1. Specimen properties

A total of six specimens, having the geometry shown in Fig. 1, were tested. Each sample consisted of a $800 \times 800 \times 50$ mm panel (shear panel) connected to four $820 \times 150 \times 200$ mm concrete chords longitudinally reinforced with #3 + 3∅16 rebars. Steel rebars (shear connectors) with a diameter of 12 mm and a length of 230 mm were cast into each chord in order to allow shear transfer between the shear panel and the chords. The shear load was applied by four hinged connections

inserted within the 46 mm-diameter through hole located in the middle of the chords. The cross-section dimensions of the chords were chosen so that its axial stiffness was suitable to ensure an almost uniform distribution of shear stress along the shear panel sides. To prove this, a preliminary study [21,22] based on finite element simulations was carried out to analyze the behavior of the panel in the elastic stage. The results showed that the shear stresses remain basically uniform, with a maximum variation of about 10% observed from the border to the centre of the panel. The free expansion or contraction of the shear panel, resulting from the deformation occurring during the test, was enabled by the joint placed between the shear panel and the chords. Such a joint consisted of a 10 mm thick Polystyrene strip placed across the shear connectors to form an open gap.

Table 1 summarizes the main properties of the specimens. Three out of six samples were characterized by a conventional reinforcement ratio (ρ_s) of 0.74% and were reinforced with 6∅8 deformed steel rebars placed both in the x- and y-direction (see Fig. 1a). The remaining three specimens were reinforced with a lower conventional reinforcement ratio ($\rho_s = 0.21\%$) obtained by placing 3∅6 deformed steel rebars both in the x- and y-direction according to the bar layout of Fig. 1b.

Two control specimens not containing steel fibers were tested. Moreover, two different volume fraction of steel fibers, i.e. 0.25% and 0.63%, corresponding respectively to a total fiber content of 20 kg/m^3 and 50 kg/m^3, were investigated. The research program adopted the same concrete matrix and steel fiber typology for all the test specimens. After casting, all specimens were stacked horizontally on the laboratory floor at room temperature till the beginning of the test. Accurate curing was needful to reduce cracking phenomena due to shrinkage as much as possible. Therefore, the panels were kept wet for at least 15 days after casting by pouring water directly on the top surface. Moreover, during the first week after casting, they were also covered with a polyethylene sheet.

3.2. Test set-up

The six specimens were cured at least for 28–30 days and then tested by the test rig schematized in Fig. 2. It consists of a steel reaction frame connected to a vertical electro-mechanical jack. To transfer the load from the jack to the specimen, a steel hinged connection provided with an axial load cell was adopted. The vertical load was converted into shear forces by four steel trusses hinged to the two top chords of the panel. The trusses were connected to the panel by steel hinges able to keep the applied forces parallel to the two sides of the panel. The same loading system was adopted to apply the shear load to the two bottom chords. A hinged connection was placed also at the bottom of the panel to transfer the shear load from the bottom trusses to the reaction frame
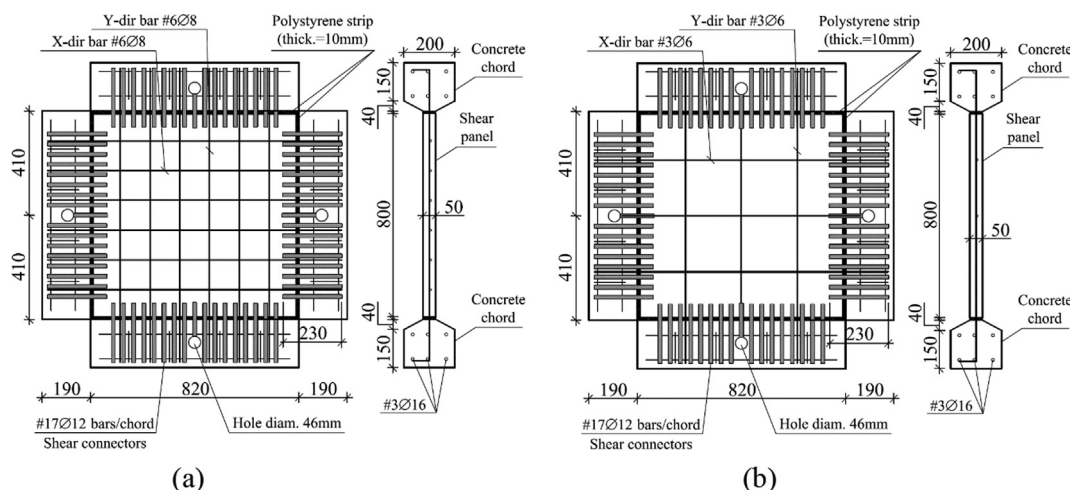
Fig. 1. Properties of the specimen series PC and FRC: panel with $\rho_s = 0.7\%$ (a); panel with $\rho_s = 0.3\%$ (b).

Table 1
Main properties of shear panels.

Panel ID	Batch ID	Reinforcing bar type	d_s, mm	$\rho_{sx} = \rho_{sy}$, %	V_f, %
SP-PC 0.21/0.0	PC-1	Ø6	6	0.21	0.0
SP-FRC 0.21/0.25	FRC0.25-1				0.25
SP-FRC 0.21/0.63	FRC0.63-1				0.63
SP-PC 0.74/0.0	PC-2	Ø8	8	0.74	0.0
SP-FRC 0.74/0.25	FRC0.25-2				0.25
SP-FRC 0.74/0.63	FRC0.63-2				0.63
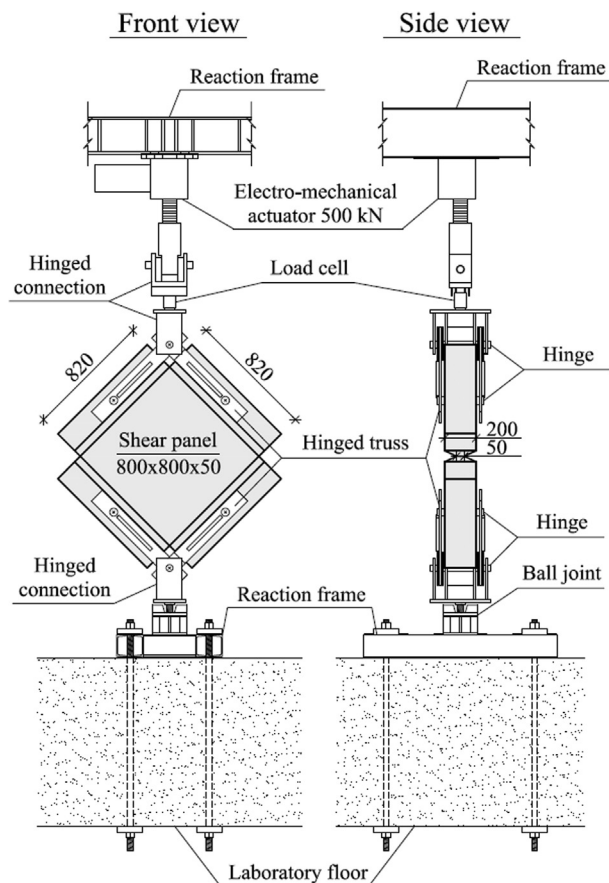
Fig. 2. Schematic of the test set-up.

anchored to the strong floor of the laboratory. Unlike the connection to the jack, a ball joint was installed between the bottom hinged connection and the reaction frame in order to minimize the effects of the load eccentricities on the structural behavior of the specimen.

The loading rate was kept constant at 5 μm/min, during the pre-cracking stage, whereas it was increased to 30 μm/min once first cracking was occurred. The load was monotonically increased till complete failure of the specimen.

3.3. Materials

The adopted concrete mixture and the steel fiber properties are reported in Table 2.

Each of the concrete batches used to cast the six panels were mechanically characterized both in tension and in compression (Table 3). The cubic compressive strength ($f_{cm,cube}$) was determined by testing 150 mm cubes under uniaxial loading after 28 days curing in a chamber at a constant temperature of 20° C and relative humidity of about 95%. The cylindrical mean compressive strength (f_{cm}) was defined as $0.83 \cdot f_{cm,cube}$, whereas the mean secant Young's modulus (E_{cm}) and the mean tensile strength (f_t) were calculated according to the Eurocode 2

[23] as $E_{cm} = 22(f_{cm}/10)^{0.3}$ and $f_t = 0.3 f_{ck}^{2/3}$.

The fracture behavior of concrete was characterized by performing 3-point bending tests (3PBTs) on $150 \times 150 \times 500$ mm notched prisms according EN 14651-5 [24]. The tests provided the nominal stress-CMOD (Crack Mouth Opening Displacement) curves of Fig. 3, as well as the limit of proportionality f_L and the residual strengths f_{R1}, $f_{R,2}$, $f_{R,3}$, $f_{R,4}$ (Table 3). The previous four residual strengths correspond to CMOD values of 0.5 mm, 1.5 mm, 2.5 mm and 3.5 mm, respectively. Note that, according to the *fib* Model Code 2010 [25], the residual strengths f_{R1} and f_{R3} are significant for serviceability and ultimate conditions, respectively.

The comparison of the two FRC batch series with the corresponding plain concrete batches (i.e. PC-1 and PC-2) shows the considerable increment of post-cracking strength and toughness provided by the adopted steel fiber contents. As expected, in spite of the higher dispersion of data related to the FRC0.63-1, the materials FRC0.63-1 and 2 presented a very similar response in terms of mean residual stresses (see Table 3). On the contrary, the batch series FRC0.25-1 was characterized by mean residual stresses 14–20% higher than those observed for the batch FRC0.25-2. Such a higher performance can be explained considering that the actual fiber content of the batch FRC0.25–1 (21 kg/m^3) was about 16% higher than that (18 kg/m^3) of the batch FRC0.25-2. This happened because of some problems occurred during casting.

Conventional steel deformed bars (B450 C according to Eurocode 2 [20]) were also used to reinforce all panels. Table 4 reports the main mechanical properties (f_y = Yield strength; f_{su} = Ultimate strength; ε_{su} = Ultimate strain) obtained by testing three samples per each type of bar according to ISO 15630–1 [26]. The Young's modulus (E_s) was assumed equal to 210 GPa.

3.4. Instrumentation

In addition to the axial load cell used to detect the total load applied to the specimen (see Fig. 2), two different detection systems were

Table 2
Concrete mixture and fiber properties.

Cement type	CEM I 42.5R
Cement content [kg/m^3]	380
Fine aggregate 0–4 mm [kg/m^3]	1082
Coarse aggregate 4–12 mm [kg/m^3]	742
Water-cement ratio	0.5
Super plasticizer (% on cement content)	0.1 (PC)
	0.1 (FRC – V_f = 0.25%)
	0.6 (FRC – V_f = 0.63%)
Fiber shape	Hooked-end
Material	High carbon, cold drawn steel
Tensile strength [MPa]	> 2200
Length l [mm]	30
Diameter Ø [mm]	0.35
Aspect ratio l/Ø	86
Fiber designation	30/0.35
Fiber view	

Table 3
Concrete mechanical properties.

Specimen	SP-PC 0.21/0.0	SP-FRC 0.21/0.25	SP-FRC 0.21/0.63	SP-PC 0.74/0.0	SP-FRC 0.74/0.25	SP-FRC 0.74/0.63
Specific gravity [kg/m³]	2450	2400	2512	2421	2489	2500
$f_{cm,cube}$ [MPa]	40.5	27.0	51.8	47.8	53.0	54.9
	(C.V. 14%)	(C.V. 7%)	(C.V. 4%)	(C.V. 17%)	(C.V. 13%)	(C.V. 14%)
f_{cm} [MPa]	33.0	22.4	43.0	40.0	44.0	45.6
f_{ck} [MPa]	27.6	16.3	37.0	34.6	39.0	37.0
f_t [MPa]	2.7	1.93	3.3	3.2	3.5	3.3
E_{cm}[a] [GPa]	31.7	28.0	34.1	33.3	34.3	34.7
Actual fiber content [kg/m³]	–	21	50	–	18	50
f_L [MPa]	4.0	3.6	5.4	3.5	4.0	5.9
	(C.V. 5%)	(C.V. 6%)	(C.V. 10%)	(C.V. 9%)	(C.V. 3%)	(C.V. 5%)
f_{R1} [MPa]	–	2.9	8.6	–	2.5	8.0
		(C.V. 13%)	(C.V. 9%)		(C.V. 10%)	(C.V. 6%)
f_{R2} [MPa]	–	3.4	8.6	–	2.7	8.0
		(C.V. 16%)	(C.V. 9%)		(C.V. 12%)	(C.V. 3%)
f_{R3} [MPa]	–	3.5	7.5	–	2.5	6.9
		(C.V. 18%)	(C.V. 11%)		(C.V. 11%)	(C.V. 5%)
f_{R4} [MPa]		3.3	6.4	–	2.3	5.9
		(C.V. 18%)	(C.V. 11%)		(C.V. 8%)	(C.V. 5%)

[a] Property determined according Eurocode 2.
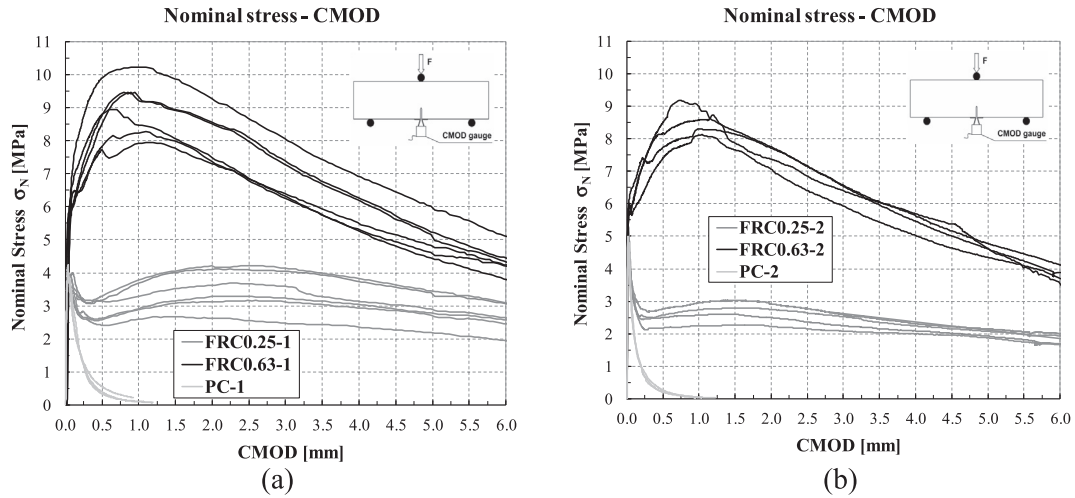
Fig. 3. Nominal stress-CMOD curves of concrete batch series (a) 1 and (b) 2.

Table 4
Properties of reinforcing steel.

Reinforcing bar type	f_y [MPa]	f_{su} [MPa]	ε_{su} [%]
Ø6	516	610	8.6
Ø8	518	620	13.1

installed to monitor the deformation on the front and the back side of the panel.

About the front side (Fig. 4a), a Digital Image Correlation (DIC) system was adopted to get comprehensive data concerning the strain state experienced by the specimen. A high resolution 50 Megapixels CMOS (Complementary Metal–Oxide–Semiconductor) sensor camera
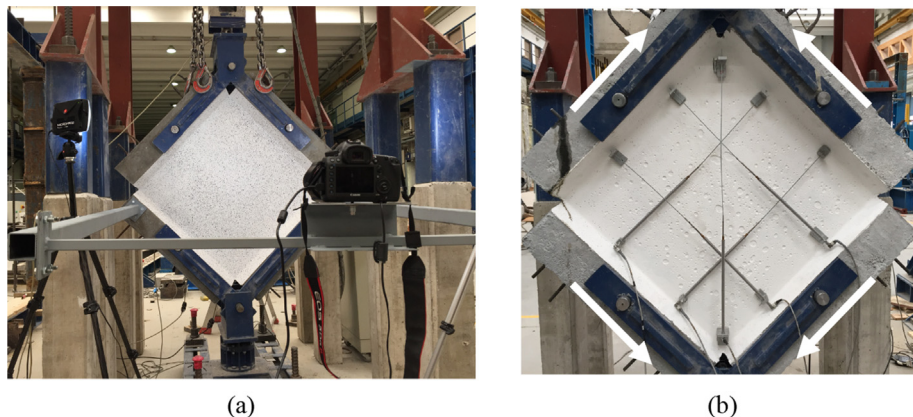
Fig. 4. View of the instrumentation on (a) front and (b) back side of the test panel.

was used to take pictures of the panel surface at 5 s intervals. In order to prevent the acquisition of spurious data resulting from rigid-body deformations of the panel, the camera was mounted on a steel frame rigidly connected to the bottom chords of the specimen (see Fig. 4a). The speckle pattern was prepared by spraying black paint on the panel surface previously painted white. In order to obtain a 2D projection of the specimen surface, the camera was placed with its optical axis normal to the specimen surface, which was lit with two led lights placed on the right and left side of the camera. To compute the displacements of the points on the coating surface, a square reference subset of about 10 × 10 pixels was chosen. Further details about the DIC method can be found in the literature [27,28].

Five Linear Variable Differential Transformers (LVDTs) were placed on the back side of the panel (Fig. 4b) to detect the deformations in the direction parallel to both the two sides and the vertical diagonal of the panel.

4. Experimental results and discussion

The tests were carried out by applying known values of the stresses ($f_x = f_y = 0$; v_{xy}) to the specimen (Fig. 5a) and by continuously detecting the strains $[\varepsilon] = [\varepsilon_x, \varepsilon_y, \gamma_{xy}]$ on the panel surface. The principal compressive (ε_2) and tensile (ε_1) strains and the corresponding direction (θ) were determined from the usual Mohr's circle of strain:

$$\varepsilon_1, \varepsilon_2 = \frac{\varepsilon_x + \varepsilon_y}{2} \pm \frac{1}{2} \bullet ((\varepsilon_x - \varepsilon_y)^2 + \gamma_{xy}^2)^{1/2} \qquad (1)$$

$$\theta = \frac{1}{2} \bullet \arctan\left(\frac{\gamma_{xy}}{\varepsilon_y - \varepsilon_x}\right) \qquad (2)$$

As suggested by Vecchio and Collins [10], who proposed a smeared crack model to study the behavior of reinforced concrete 2D elements (MCFT), the equilibrium of the panel results from the following equations:

$$f_x = f_{cx} + \rho_x \cdot f_{sx} \qquad (3)$$

$$f_y = f_{cy} + \rho_y \cdot f_{sy} \qquad (4)$$

$$v_{xy} = v_{cxy} \qquad (5)$$

where f_{cx}, f_{cy} and v_{cxy} are the average concrete stresses; ρ_x and ρ_y are the reinforcement ratios in the x and y-direction, respectively; f_{sx} and f_{sy} are the average stresses acting in the x and y reinforcement, respectively. Considering perfect steel-to-concrete bond, average axial deformations of rebars (ε_{sx}, ε_{sy}) were calculated from the measured strain in the surrounding concrete, i.e. $\varepsilon_{sx} = \varepsilon_x$ and $\varepsilon_{sy} = \varepsilon_y$. To relate axial reinforcement strain and stresses, the typical elastic-perfect plastic constitutive law was considered. Therefore:

$$f_{sx} = E_s \cdot \varepsilon_{sy} \leqslant f_{yx} \qquad (6)$$

$$f_{sy} = E_s \cdot \varepsilon_{sx} \leqslant f_{yy} \qquad (7)$$

where E_s is the Young's modulus of reinforcing steel; f_{yx} and f_{yy} are the yielding strengths of x and y reinforcement, respectively. Knowing the reinforcement stresses and the stresses applied to the panel, concrete stresses were determined from the equilibrium Eqs. (3)–(5). Finally, principal concrete stresses (f_{c2}, f_{c1}) were determined from the Mohr's circle of stresses (Fig. 5b). Fig. 6 shows the strain and stress circles for the specimen SP-FRC 0.21/0.25. Note that compression stress and strain quantities are negative.

All the key parameters detected during the tests (or calculated) are summarized in Table 5.

4.1. Stress-strain response of the panels

Fig. 7 reports and compare, for all specimens, the shear stress (v_{xy})-shear strain (γ_{xy}) curves as well as the principal tensile stress ($f_{c1}/f_{c1,cr}$)-principal tensile strain (ε_1) response normalized with respect to the tensile cracking strength ($f_{c1,cr}$).

In more detail, the response of the test panels provided with a reinforcement ratio of 0.74% is depicted in Fig. 7a. As one may observe, the specimens SP-PC 0.74/0.0 and SP-FRC 0.74/0.63 exhibited an initial stiffness significantly lower than that of the specimen SP-FRC 0.74/0.25. Such a stiffness reduction in the elastic stage can be explained considering the shrinkage cracks observed especially on one of the two sides of the panels before testing. Excessive shrinkage was probably due to faulty curing operations performed during the storage period. Shrinkage cracks may also explain the reduced value (-20%) of both the first cracking shear ($v_{xy,cr}$) and the tensile ($f_{c1,cr}$) strengths that characterized the specimens SP-PC 0.74/0.0 and SP-FRC 0.74/0.63 with respect to those of the panel SP-FRC 0.74/0.25. After first cracking, the second branch of the v_{xy}-γ_{xy} response presented different slopes depending on the total content of steel fibers. In fact, compared to the reference specimen SP-PC 0.74/0.0 not containing fibers, the panel (SP-FRC 0.74/0.63) reinforced with the highest fiber content ($V_f = 0.63\%$) exhibited more pronounced tension stiffening stresses leading to a higher strength of the specimen. On the contrary, the lower fiber content (0.25%) used in the panel SP-FRC 0.74/0.25 had a less significant effect on the tensile behavior, which appeared to be closer to that observed for the reference specimen. The $f_{c1}/f_{c1,cr}$-ε_1 diagram of Fig. 7c clearly supports the previous considerations on the tensile
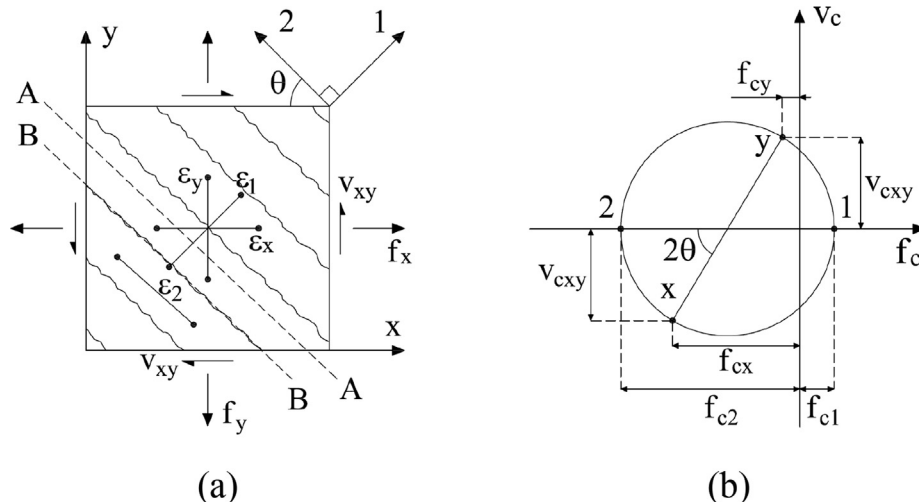
Fig. 5. Equilibrium conditions of a plane-stress element: (a) Applied stresses and strains; (b) Mohr's circle of average stresses in concrete.
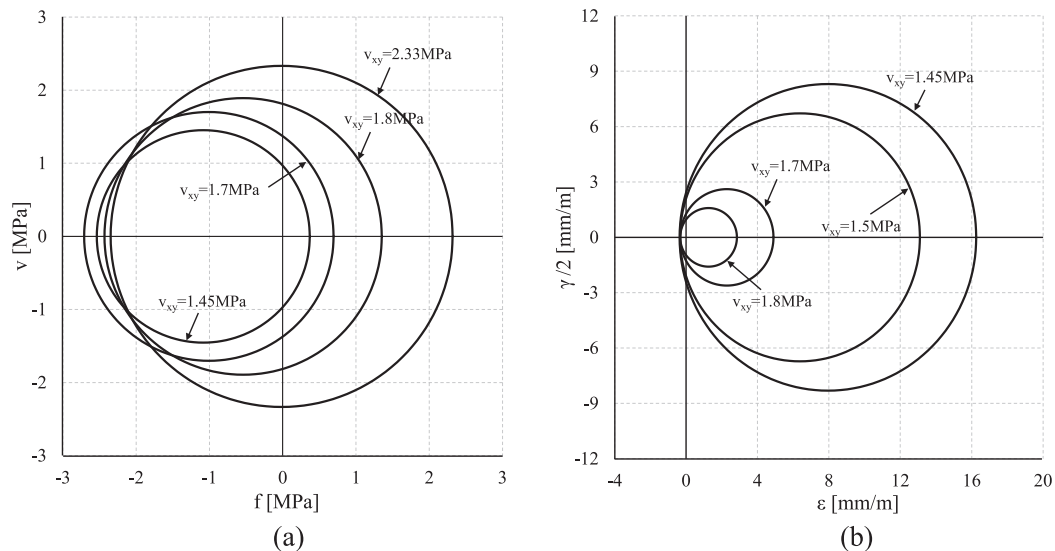
Fig. 6. Mohr's circles of average stresses (a) and strains (b) determined for the panel SP-FRC 0.21/0.25.

behavior. Indeed, after cracking, the principal tensile stresses of the panel SP-FRC 0.74/0.63 remain permanently higher than those exhibited by the other two panels. However, the low fiber content adopted in the panel SP-FRC 0.74/0.25 had a beneficial effect on its post-cracking tensile response, which appears more stable and linear compared to the "wobbly" response of the reference specimen.

As expected, at the onset of bi-axial yielding of rebars, the slope of the v_{xy}-γ_{xy} curves progressively decreased and the residual tensile strength was mainly governed by tension softening of concrete. The latter was clearly more significant for the samples SP-FRC 0.74/0.25 and SP-FRC 0.74/0.63, which showed a shear strength respectively 9% and 15% higher than the one observed for the reference panel. The $f_{c1}/f_{c1,cr}$-ε_1 diagram (Fig. 7c) allows also stating some considerations about the effect of the different fiber contents on tension stiffening. In fact, compared to the specimen SP-FRC 0.74/0.25, the normalized tensile strength presented by the panel SP-FRC 0.74/0.63 was significantly higher especially in the strain range 1.4–6.0 mm/m, where the increment of the normalized strength varied from a minimum of +40% to a maximum of +270%. Therefore, the use of a higher fiber content considerably improved the tension stiffening effect and led to a more stable progression of the cracking process.

The responses of the specimens having a reinforcement ratio of 0.21% are shown in Fig. 7b and d. As one may expect, the very low content of steel reinforcement caused a softening response after cracking that led to a reduction of both shear and principal tensile strength. Unfortunately, the comparison of the three panels cannot be fully performed as the sample SP-PC 0.21/0.0 experienced a very brittle shear failure right after concrete first cracking. Thus, the diagrams of Fig. 7b and d only report the first linear branch detected during the test of the reference specimen. The v_{xy}-γ_{xy} responses of the two FRC panels appear quite different (Fig. 7b), especially for shear strain values lower than 15 mm/m. After first cracking, the panel SP-FRC 0.21/0.25 showed a sharp decrease of the shear resistance that was effectively controlled by the presence of fibers in the concrete matrix. Then, the shear stress gradually decreased up to complete failure of the specimen that occurred at total shear strain of about 20.2 mm/m because of tensile rupture of rebars. Compared to the specimen SP-FRC 0.21/0.25, the first cracking shear strength of the panel SP-FRC 0.21/0.63 was about 34% higher. Therefore, the post-cracking response of the two samples cannot be directly compared as the considerably different values of the cracking strength would necessarily affect the results. However, the curves allow appreciating how the higher fiber content used in the panel SP-FRC 0.21/0.63 led to a better crack control since

the first loading stages after cracking. Furthermore, the shear stress (v_{xy} = 2.24 MPa) corresponding to the bi-axial yield of rebars was 30% higher than that observed for the specimen SP-FRC 0.21/0.25. Failure of the panel SP-FRC 0.21/0.63 occurred at a shear strain of 18.6 mm/m (rebars rupture).

The $f_{c1}/f_{c1,cr}$-ε_1 diagram of Fig. 7d better highlights the actual structural performance provided by the different fiber dosages adopted. Contrary to expectation, the higher fiber content of panel SP-FRC 0.74/0.63 led to a limited increment (+40%) of the normalized strength. Moreover, after rebars yielding, the response of specimen SP-FRC 0.74/0.63 progressively decreased up to the minimum value achieved by specimen SP-FRC 0.74/0.21.

From the previous considerations, one may conclude that the use of fiber improves the tensile strength related to the tension stiffening mechanism. However, the combined effect of fibers and rebars appears to be more effective in case a higher reinforcement ratio (ρ_s = 0.74%) is adopted. Thus, unlike many analytical models [9,29,30,31,32], when modelling the tension stiffening effect, it is suggested to take into account the influence of the effective conventional reinforcement ratio.

Table 5 reports also information about the principal compressive stress ($f_{c2,u}$) detected at failure. As one may note, the use of fiber did not significantly affect the compressive response at failure as the stresses detected appear to be quite similar for the samples having the same conventional reinforcement ratio. Fibers would affect more the compression regime in the case higher stresses and deformation in compression would be reached (i.e., with higher reinforcement ratios).

4.2. Crack width and crack spacing

An important feature that allows to further understand the experimental results is the evolution of the crack pattern and the corresponding variation of the mean crack spacing (s_m). The latter was here calculated as the mean distance between cracks progressively detected during test execution.

About the panels with a reinforcement ratio of 0.74%, the failure patterns (Fig. 8) observed at the end of the tests presented a significant number of cracks oriented at a constant inclination of 45° with respect to the x-y reference system. The evolution of crack spacing is well represented by the average crack spacing – shear stress curves of Fig. 9a. By increasing the applied shear stress, the crack spacing of the three samples tended to decrease up to the minimum values ($s_{m,min}$) reported in Table 5. The advantage provided by fibers is well highlighted by the response of the specimen SP-FRC 0.74/0.63, whose minimum crack

Table 5
Summary of main experimental results.

Specimen	f_{cm} [MPa]	$v_{xy,cr}$ [MPa]	$\gamma_{xy,cr}$ [mm/m]	$v_{xy,max}$ [MPa]	$\gamma_{xy,max}$ [mm/m]	$\gamma_{xy,u}$ [mm/m]	$v_{xy,u}$ [MPa]	$\varepsilon_{x,u}$ [mm/m]	$\varepsilon_{y,u}$ [mm/m]	$s_{m,min}$ [mm]	$w_{m,max}$ [mm]	$f_{c1,cr}$ [MPa]	$f_{c2,u}$ [MPa]	Failure mode
SP-PC 0.74/0.0	33.6	2.5	1.26	4.6	40.00	40.00	4.6	18.10	17.20	85	3.0	2.5	−8.2	Bi-axial yield of rebars - rebars rupture
SP-FRC 0.74/0.25	22.4	3.4	0.57	4.9	29.88	29.88	4.9	13.00	14.20	85	2.4	3.7	−8.8	Bi-axial yield of rebars - rebars rupture
SP-FRC 0.74/0.63	43.0	2.66	1.70	5.4	40.00	40.00	5.3	16.5	17.5	66	3.0	2.6	−9.3	Bi-axial yield of rebars - rebars rupture
SP-PC 0.21/0.0	40.0	3.1	0.15	3.1	0.15	0.15	3.1	0.03	−0.05	425	–	3.1	−3.0	Brittle failure at 1st cracking
SP-FRC 0.21/0.25	44.0	2.3	0.14	2.3	0.14	20.20	1.0	10.60	12.20	282	5.8	2.3	−2.1	Bi-axial yield of rebars - rebars rupture
SP-FRC 0.21/0.63	45.6	3.1	0.11	3.1	0.11	18.60	1.1	10.00	7.21	120	2.2	3.1	−2.2	Bi-axial yield of rebars - rebars rupture

– value non detected.

spacing was 22% lower than that detected for the reference specimen. Contrary to what expected, the panel reinforced with the lowest content of fibers (SP-FRC 0.74/0.21) presented a final crack spacing equal to the reference specimen one. This fact confirms the previous observations concerning the limited effect of the very low contents of fibers on tension stiffening.

The ultimate crack patterns of the panels with a reinforcement ratio of 0.21% (Fig. 8) were characterized by cracks with an inclination of 45° to the reference axes x-y. However, because of the very low conventional reinforcement ratio, few localized cracks were observed on the panel surface. The reference panel (SP-PC 0.21/0.0) collapsed once a single crack occurred close to the main diagonal of the panel. The addition of 20 kg/m^3 to concrete (SP-FRC 0.21/0.25) slightly reduced the average crack spacing (Fig. 9b) leading to the localization of a main crack running along the panel diagonal and of a secondary crack located close to the top corner of the specimen. As shown in Fig. 9b, the specimen SP-FRC 0.21/0.63 exhibited a higher number of cracks that allowed to significantly reduce the final crack spacing ($s_{m,min}$).

By multiplying the average crack spacing by the principal tensile strain (Eq. (8)), the average crack width (w_m) values shown in the diagrams of Fig. 9 were determined. It is seen that irrespective of the reinforcement ratio adopted, the higher is the fiber content, the higher is the shear strength of the specimen compared to that of the reference panel under the same crack width. This fact is related to the ability of FRC to provide a better control of the cracks growth. Considering the panels having a reinforcement ratio of 0.74% (Fig. 9a), the best crack control was performed by the specimen SP-FRC 0.74/0.63, whose shear resistance detected in the crack width range 0.5–0.8 mm was about 25% and 45% higher than those exhibited by the specimens SP-FRC 0.74/0.25 and SP-PC 0.74/0.0, respectively. Anyway, the specimen with the lowest fiber content (SP-FRC 0.74/0.25) presented a good ability to control the cracking evolution as its shear resistance (see the range of shear stresses v_{xy} = 4–5 MPa) was appreciably higher than that of the reference sample. The specimens with the lower reinforcement ratio (Fig. 9b), were characterized by a softening behavior after cracking that favoured the formation of cracks larger than the ones shown in Fig. 9a. Compared to the sample SP-FRC 0.21/0.25, the panel SP-FRC 0.21/0.63 showed a better ability to control the crack growth especially right after first cracking (i.e., crack width range 0–0.6 mm). However, for values of the applied shear stress lower than 1.75 MPa, panel SP-FRC 0.21/0.25 exhibited a continuous increase of the crack width under an almost constant shear stress, until rebars rupture occurred. On the contrary, specimen SP-FRC 0.21/0.63 presented a less pronounced increase of the average crack width, which achieved a maximum value at failure ($w_{m,max}$) significantly lower than that observed for the specimen SP-FRC 0.21/0.63 (Table 5).

5. Prediction of crack spacing

Smeared crack models used for predicting the response of bi-dimensional concrete elements frequently consider stress-crack width constitutive relationships to represent the tensile behavior of concrete. According to Vecchio and Collins [10], the average crack width (w_m) can be estimated by the following simple equation:

$$w_m = \varepsilon_1 \cdot s_{m\theta} \tag{8}$$

in which w_m is related to both the average concrete principal tensile strain (ε_1) and the average crack spacing ($s_{m\theta}$). Once the crack spacing in the reference x ($s_{mx,FRC}$) and y ($s_{my,FRC}$) directions of the FRC panel are known, the average crack spacing in the FRC panel can be calculated as follows:

$$s_{m\theta} = \left(\frac{\sin\theta}{s_{mx,FRC}} + \frac{\cos\theta}{s_{my,FRC}} \right)^{-1} \tag{9}$$

To predict the average crack spacing in a reinforced concrete 2D
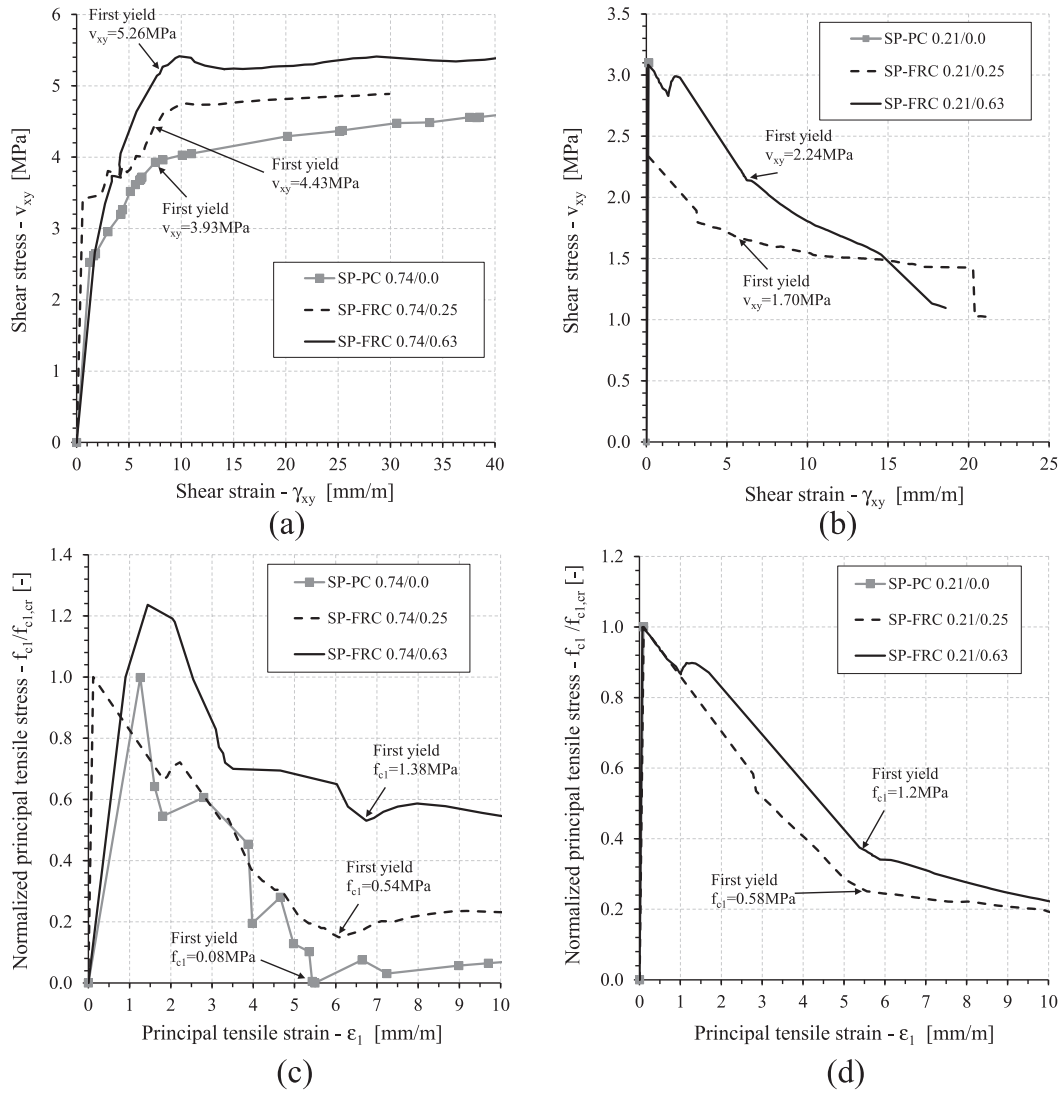
Fig. 7. Shear stress (v_{xy})-shear strain (γ_{xy}) response and normalized principal tensile stress (f_{c1})-principal tensile strain (ε_1) response of the test panels: (a) v_{xy}-γ_{xy} for panels with $\rho_{sx} = \rho_{sy} = 0.74\%$; (b) v_{xy}-γ_{xy} for panels with $\rho_{sx} = \rho_{sy} = 0.21\%$; (c) normalized f_{c1}-ε_1 for panels with $\rho_{sx} = \rho_{sy} = 0.74\%$; (d) normalized f_{c1}-ε_1 for panels with $\rho_{sx} = \rho_{sy} = 0.21\%$.

continuum, the following expressions were proposed by the CEB-FIP Model Code 1978 [33] code:

$$s_{mx} = 2 \cdot \left(c_x + \frac{d_x}{10} \right) + \frac{1}{4} \cdot k_1 \cdot \frac{\varnothing_x}{\rho_x} \tag{10}$$

$$s_{my} = 2 \cdot \left(c_y + \frac{d_y}{10} \right) + \frac{1}{4} \cdot k_1 \cdot \frac{\varnothing_y}{\rho_y} \tag{11}$$

where

c_x, c_y are the largest diagonal distances between any point in the concrete and a bar oriented in the x and y direction, respectively [26,34];
d_x, d_y are the spacings between bars placed in the x and y direction, respectively;
$k_1 = 0.4$ for deformed bars or 0.8 for plain bars or bonded strands;
$\varnothing_x$, $\varnothing_y$ are the diameters of the bars in the x and y direction, respectively;
ρ_x, ρ_y are the reinforcement ratios in the x and y direction, respectively.

Note that in case no conventional reinforcement is provided in

either one or both directions, crack spacing can be assumed equal to ten times the element thickness [31].

In order to take into account the effect of fibers on crack spacing, nominal crack spacings s_{mx} and s_{my} were reduced by the correction factor originally proposed by Moffat [28], which was here conveniently adjusted to include the dependency from the residual strength f_{R1} of FRC. Thus

$$s_{mx,FRC} = (1 - 0.25 \cdot f_{R1}/f_t) \cdot s_{mx} \geqslant 0.2 \cdot s_{mx} \tag{12}$$

$$s_{my,FRC} = (1 - 0.25 \cdot f_{R1}/f_t) \cdot s_{my} \geqslant 0.2 \cdot s_{my} \tag{13}$$

In the previous equations, in order to have a positive value, the term $0.25 f_{r1}/f_t$ should be lower than 1. In addition, a lower bound ($\geqslant 0.2 s_m$) was introduced to limit the minimum value of the resulting crack spacing, also supported by the results of an extensive experimental program on cracking of FRC tension ties [35,37]. The reliability of the crack spacing formulation reported above was assessed by predicting the response of some FRC elements including the four panels tested herein, two panels tested by Susetyo et al. [13] and six tie-elements tested by Tiberti et al. [32]. The main parameters used in the prediction are reported in Table 6. Note that the mean tensile strengths (f_t) reported in the table were calculated according to the Eurocode 2 [23]

SP-PC 0.74/0.0

SP-FRC 0.74/0.25

SP-FRC 0.74/0.63

SP-PC 0.21/0.0

SP-FRC 0.21/0.25

SP-FRC 0.21/0.63
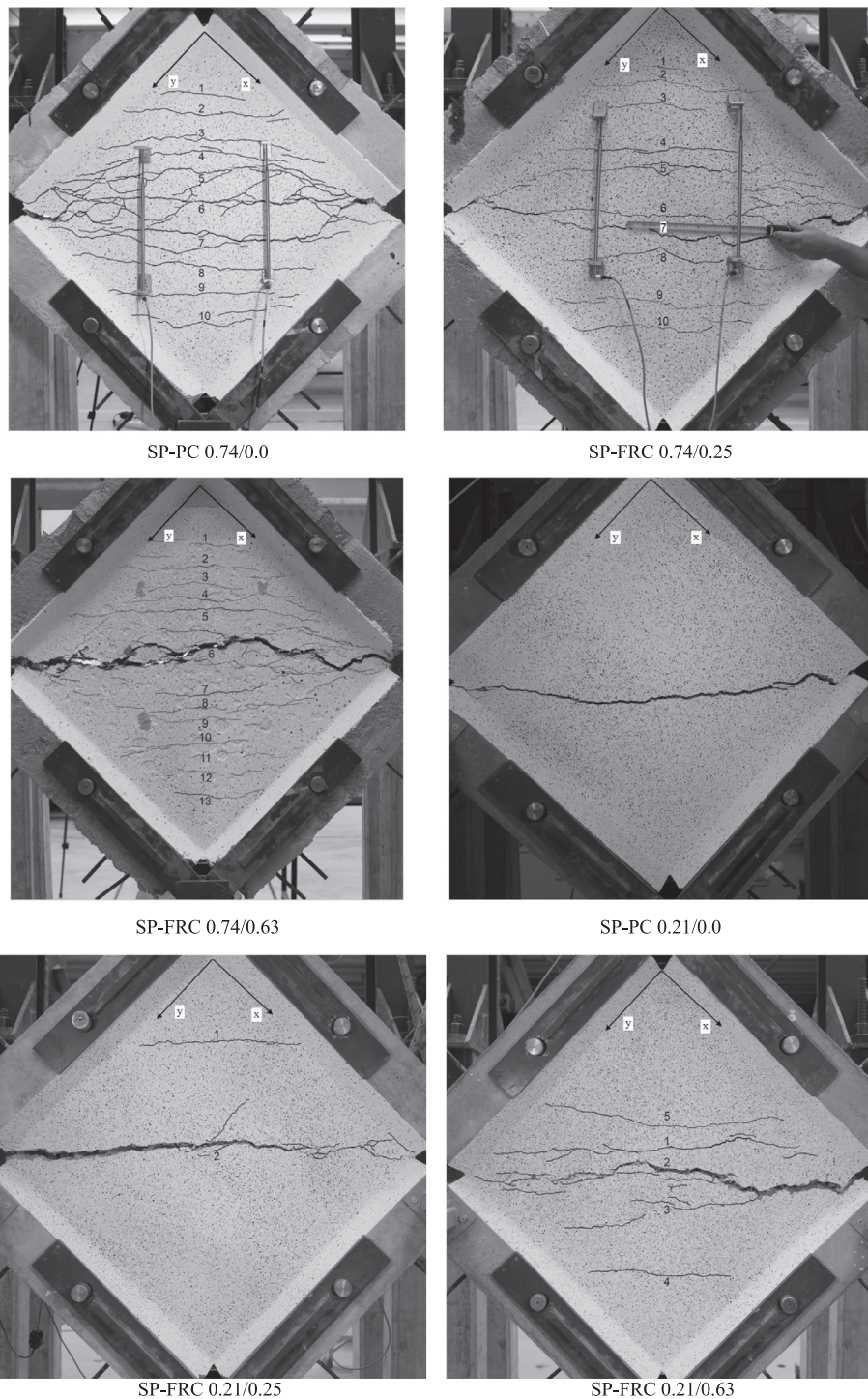
Fig. 8. View of the failure patterns observed at the end of the tests.

(i.e., $f_t = 0.3f_{ck}^{2/3}$) whereas the angle θ used for the FRC panels was obtained by averaging the angles detected in the post-cracking experimental response.

Fig. 10 compares the experimental crack spacing with that predicted by the equations (12) and (13). It is worth remarking that the crack spacing of FRC panels considered in the comparison corresponded to that measured at the end of tests. In fact, FRC panels achieved the stabilized crack spacing when the average crack width was approximately equal to 0.5 mm. This fact was clearly highlighted also by data reported by Susetyo [38] as well as by the diagrams of Fig. 9, which illustrate a stable crack spacing for average crack widths ranging from

0.5 mm to 0.8 mm. Therefore, the experimental results are consistent with the adoption of predicting equations based on the residual strength f_{R1}, for a value of CMOD = 0.5.

The low values of the MPE (Mean Percentage Error) and of the MAPE (Mean Absolute Percentage Error) prove the quite good agreement between the experimental and the predicted crack spacing.

6. Conclusions

Six tests on FRC panels under pure shear were presented and discussed in this paper. Based on the experimental results and on the
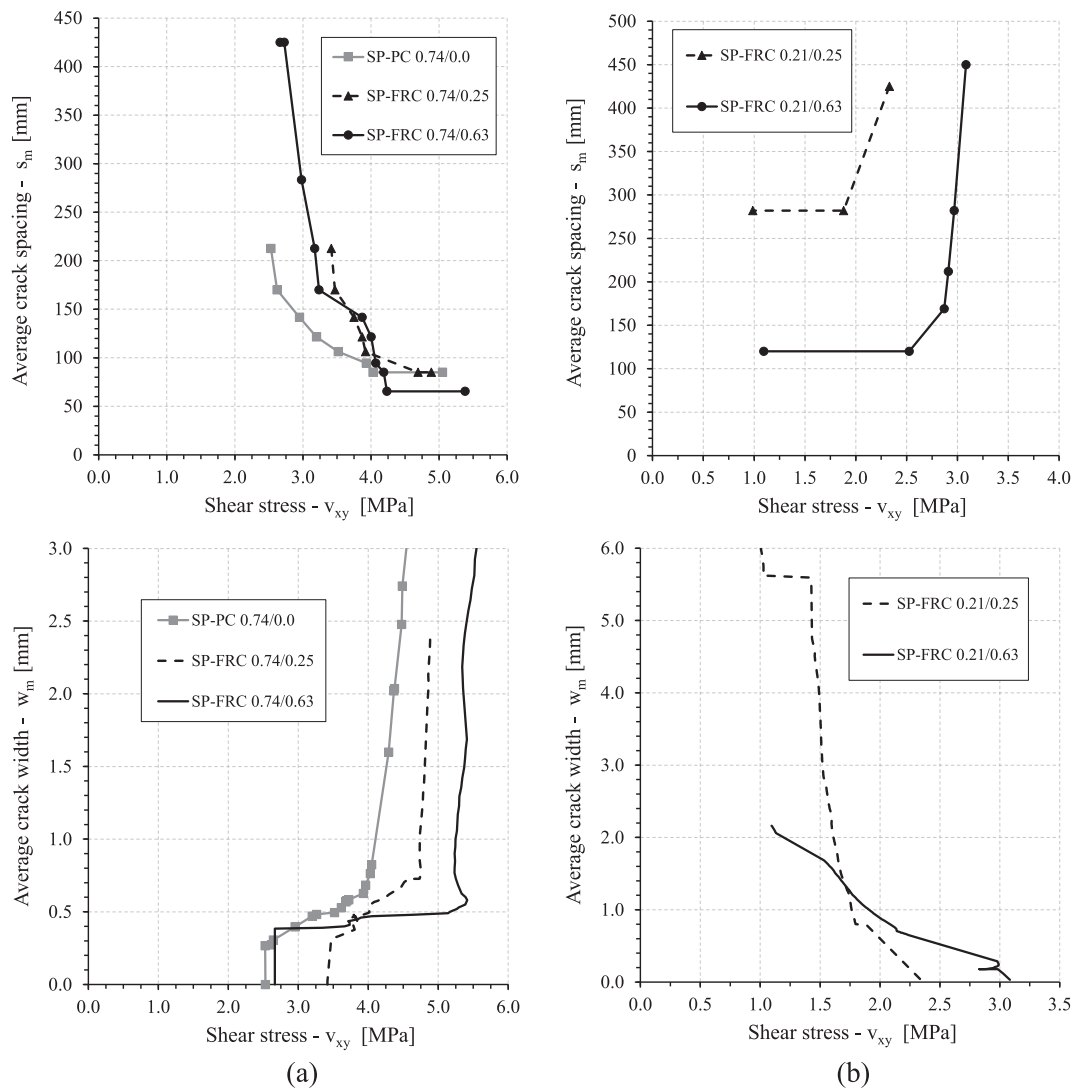
Fig. 9. Comparison of experimental average crack spacing (s_m)-shear stress (v_{xy}) and average crack width (w_m)-shear stress (v_{xy}) response of the test panels: (a) panels with $\rho_{sx} = \rho_{sy} = 0.74\%$; (b) panels with $\rho_{sx} = \rho_{sy} = 0.21\%$.

following discussion, the following main conclusions can be drawn:

- FRC significantly affects the behavior of panels with higher steel reinforcement, in terms of shear strength and stiffness right after first cracking. In fact, tension stiffening appeared more pronounced in the FRC panels than in the reference panel without fibres. This is due to the increased residual strength promoted by the use of fibre.
- By comparing the shear strength of the panels with the highest conventional reinforcement ratio, significant differences were observed for crack width values higher than 0.5 mm. In fact, considering the crack width rang 0.5–0.8 mm, the shear strength of the panels containing 0.25% and 0.63% of fibers was respectively 25% and 40% higher than that achieved by the reference specimen.
- The FRC panels with a low reinforcement ratio presented a softening response after cracking. However, fibers allowed to control the post-peak stage leading to a stable and progressive reduction of the shear strength for increasing shear deformations.
- The use of low amounts of rebars made the principal tensile stress–strain response of the two specimens (SP-FRC 0.21/0.25, SP-FRC 0.21/0.63) very similar after cracking. Small differences were detected only for relatively small levels of cracking (w = 0–0.6 mm), for which the panel with the highest fiber dosage better performs. In general, higher volume fractions of fibers should

be utilized with low amounts of rebars.
- The tension stiffening effect appeared to be related to the actual amount of rebars. Thus, as recommended by others [34], when formulating models for predicting the tension stiffening effect, the effective conventional reinforcement ratio should be taken into account.
- An adaptation of a well-known formulation for the crack spacing was herein proposed in the case of FRC, based on the fiber performance at serviceability limit states (residual strength f_{R1}); the comparison against the results herein reported and those collected in literature proves the reliability of the proposed model. However, the latter should be further evaluated with a broader set of experiments, when available.

Finally, it is worth remaking that the conclusions above stated can be generally extended only to normal strength FRC containing hooked-end steel fibers. Additional tests should be carried out to assess their applicability to FRCs containing other types of fibers (e.g., polypropylene fibers, glass fibers, etc.). The present conclusions cannot be certainly extended to Ultra High Performance Fiber Reinforced Concrete, whose typical uniaxial tensile strain-hardening behavior is different compared to the softening response exhibited by the materials adopted in this study.

Table 6
Parameters implemented in the proposed crack spacing model.

	Specimen	c_x [mm]	c_y [mm]	d_x [mm]	d_y [mm]	$\emptyset_x$ [mm]	$\emptyset_y$ [mm]	ρ_x [%]	ρ_y [%]	f_{Rt} [MPa]	f_t [MPa]	θ [°]	$s_{x,FRC}$ [mm]	$s_{y,FRC}$ [mm]	$s_{m\theta}^*$ [mm]	$s_{m\theta}^{**}$ [mm]
Tested panels	SP-FRC 0.74/0.25	62	62	117	117	8	8	0.74	0.74	2.5	3.5	47	209	209	148	85
	SP-FRC 0.74/0.63	62	62	117	117	8	8	0.74	0.74	8.0	3.3	49	102	102	72	86
	SP-FRC 0.21/0.25	104	104	203	203	6	6	0.21	0.21	2.9	2.7	46	334	334	236	282
	SP-FRC 0.21/0.63	104	104	203	203	6	6	0.21	0.21	8.6	3.4	44	195	195	138	120
Susetyo et. al. [13]	C1F1V1	26	26	29	0	8	0	3.3	0	5.8	3.7	36	50	700	96	114
	C1F2V3	26	26	29	0	8	0	3.3	0	15.6	4.2	38	16	140	23	38
Tiberti et al. [32]	N80/10-0.5M	35	35	0	0	10	0	1.25	0	4.1	3.4	0	104	0	104	104
	N80/10-1M	35	35	0	0	10	0	1.25	0	5.4	2.9	0	79	0	79	79
	N120/20-0.5M	50	50	0	0	20	0	2.23	0	4.1	3.4	0	131	0	131	131
	N120/20-1M	50	50	0	0	20	0	2.23	0	5.4	2.9	0	99	0	99	99
	N180/20-0.5M	80	80	0	0	20	0	0.98	0	4.1	3.4	0	252	0	252	252
	N180/20-1M	80	80	0	0	20	0	0.98	0	5.4	2.9	0	191	0	191	191
	N180/30-0.5M	75	75	0	0	30	0	2.23	0	4.1	3.4	0	197	0	197	197
	N180/30-1M	75	75	0	0	30	0	2.23	0	5.4	2.9	0	149	0	149	149
	N200/30-0.5M	85	85	0	0	30	0	1.8	0	4.1	3.4	0	233	0	233	233
	N200/30-1M	85	85	0	0	30	0	1.8	0	5.4	2.9	0	176	0	176	176

$s_{m\theta}^*$: predicted value of the average crack spacing.
$s_{m\theta}^{**}$: experimental value of the average crack spacing.
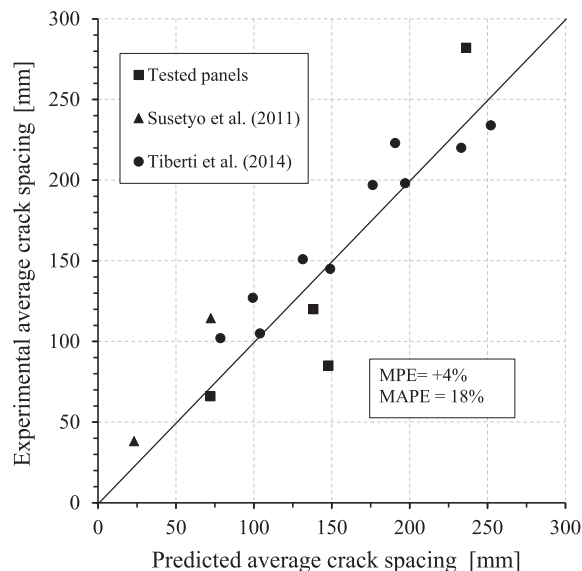
Fig. 10. Experimental and predicted average crack spacing comparison.

Declaration of competing interest

The authors declare that there is no conflict of interest.

Acknowledgments

Appendix A. Supplementary material

Supplementary data to this article can be found online at https://doi.org/10.1016/j.engstruct.2019.109879.

References

[1] Li VC, Ward R, Hamza AM. Steel and synthetic fibers as shear reinforcement. ACI Struct J 1992;89(5):499–508.

[2] Adebar P, Mindess S, St.-Pierre D, Olund B. Shear tests of fiber concrete beams without stirrups. ACI Struct J 1997;94(1): 68–76.

[3] Kwak YK, Eberhard MO, Kim WS, Kim J. Shear strength of steel fiber-reinforced concrete beams without stirrups. ACI Struct J 2002;99(4):530–8.

[4] Parra-Montesinos G, Wight JK, Dinh H, Libbrecht A, Padilla C. Shear strength of fiber reinforced concrete beams without stirrups. Report No. UMCEE 06-04, University of Michigan, Ann Arbor, MI; 2006. 39 pp.

[6] Minelli F, Plizzari GA. On the effectiveness of steel fibers as shear reinforcement. ACI Struct J 2013;110(3):379–89.

[8] Facconi L, Minelli F, Plizzari G, Ceresa P. Experimental study on steel fiber reinforced concrete beams in pure torsion. In: Proc of the fib Symposium in Krakow, 27-29 May, 2019, Krakow, Poland. n° 47 - Concrete Innovations in Materials, Design and Structures. Edited by: Wit Derkowski et al., p. 513–4 ISBN: 978-2-940643-01-1.

[9] Vecchio FJ, Collins MP. The response of reinforced concrete to in-plane shear and normal stresses. Publication No. 82–03, Department of Civil Engineering. University of Toronto; 1982. p. 332.

[10] Vecchio FJ, Collins MP. The modified compression-field theory for reinforced concrete elements subjected to shear. ACI J 1986;83(2):219–31.

[11] Zhang LXB, Hsu TT. Behavior and analysis of 100 MPa concrete membrane elements. J Struct Eng 1998;124(1):24–34.

[12] Bosiljkov VZ, Totoev YZ, Nichols JM. Shear modulus and stiffness of brickwork masonry: an experimental perspective. Struct Eng Mech 2005;20(1):21–44.

[13] Susetyo J, Gauvreau P, Vecchio FJ. Effectiveness of steel fiber as minimum shear reinforcement. ACI Struct J 2011;108(4):488–96.

[14] Carnovale D, Vecchio FJ. Effect of fiber material and loading history on shear behavior of fiber-reinforced concrete. ACI Struct J 2014;111(5):1235–44.

[15] Chasioti SG, Vecchio FJ. Shear behavior and crack control characteristics of hybrid steel fiber-reinforced concrete panels. ACI Struct J 2017;114(1):209–20.

[16] Holschemacher K, Iskhakov I, Ribakov Y, Mueller T. Laboratory tests of two-layer beams consisting of normal and fibered high strength concrete: ductility and technological aspects. Mech Adv Mater Struct 2012;19(7):513–22.

[18] Facconi L, Plizzari G, Minelli F. Elevated slabs made of Hybrid Reinforced Concrete: proposal of a new design approach in flexure. Struct Concr 2019;20(1):52–67. doi:10.0.3.234/suco.201700278.

[19] Pujadas P, Blanco A, De la Fuente A, Aguado A. Cracking behavior of FRC slabs with traditional reinforcement. Mater Struct 2012;45(5):707–25.

[20] Facconi L, Minelli F, Plizzari G. Steel fiber reinforced self-compacting concrete thin slabs – experimental study and verification against Model Code 2010 provisions. Eng Struct 2016;122: 226–237. 10.1016/j.engstruct.2016.04.030.

[21] Moser M. Prove sperimentali a taglio puro su materiali fragili", Master Thesis, Department of Civil, Environmental, Architectural Engineering and of Mathematics, Università di Brescia, Italy; 2013 [in Italian].

[22] Coccoli L. Elementi in calcestruzzo fibrorinforzato soggetti a taglio puro. Master Thesis, Department of Civil, Environmental, Architectural Engineering and of Mathematics, Università di Brescia, Italy; 2018 [in Italian].

[23] EN 1992-1-1: Eurocode 2. Design of Concrete Structures. Part 1-1: General rules and rules for buildings; 2005.

[24] EN 14651-5. Precast concrete products – test method for metallic fibre concrete – Measuring the flexural tensile strength, European Standard; 2005.

[25] fib Model Code for Concrete Structures 2010. October 2013. 434 pages. ISBN: 978-3-433-03061-5.

[26] ISO 15630-1. Steel for the reinforcement and prestressing of concrete - Test methods – Part 1: Reinforcing bars, wire rod and wire; 2010.

[27] Pan B, Qian K, Xie H, Asundi A. Two-dimensional digital image correlation for in-plane displacement and strain measurement: a review. Meas Sci Technol 2009;20: 062001, 17pp.

[28] Pease BJ, Stang H, Geiker MR, Weiss WJ. Photogrammetric assessment of flexure induced cracking of reinforced concrete beams under service loads. In: Proceedings of the 2nd international RILEM symposium, advances in concrete through science and engineering, Quebec City, Canada; 2006.

[29] Collins MP, Mitchell D. Prestressed concrete structures. Canada: Response publications; 1997. p. 756.

[30] Tamai S, Shima H, Izumo J, Okamura H. Average stress-strain relationship in post yield range of steel bar in concrete. Concr Library JSCE 1987;11:117–29.

[31] Moffatt K. Analyse de Dalles de Pont avec Armature Réduite et Béton de Fibres Metalliques", M.Sc.A. Thesis, École Polytechnique de Montréal; 2001. p. 248.

[32] Bischoff PH. Tension stiffening and cracking of steel fiber-reinforced concrete. ASCE J Mater Civil Eng 2003; 15(2): p. 174–82.

[33] Comité Euro-Internationale du Béton, CEB-FIP Model Code 1978 — Design Code, Comité Euro-International du Béton, CEB Bulletin d' Information No. 124/125. Thomas Telford, London; 1978.

[34] Bentz EC. Sectional analysis of reinforced concrete members. Ph.D. Thesis, Department of Civil Engineering, University of Toronto; 2000, 198 pp.

[35] Tiberti G, Minelli F, Plizzari G. Cracking behavior in reinforced concrete members with steel fibers: a comprehensive experimental study. Cem Concr Res 2015;68:24–34.

[37] Minelli F, Tiberti G, Plizzari GA. Crack control in RC elements with fiber reinforcement. paper ID: SP-280-6; ACI Special Publication ACI SP-280: Advances in FRC Durability and Field Applications CD-ROM, Vol. 280, Editors: Corina-Maria Aldea & Mahmut Ekenel; December 2011, pp. 18. ISBN 0-87031-751-2 and/or 978-0-87301-751-4.

[38] Susetyo J. Fibre reinforcement for shrinkage crack control in prestressed, precast segmental bridges. Ph.D. thesis, Department of Civil Engineering. University of Toronto; 2009.